Am J Transl Res 2025;17(2):941-950
www.ajtr.org /ISSN:1943-8141/AJTR0160463

Original Article

A nomogram predicts the new high-grade patterns of pulmonary invasive non-mucinous adenocarcinoma based on the radiomics and clinical features

Ruxin Shen[1], Zhaoshui Li[1], Yingying Zhang[2]

[1]Qingdao Medical College, Qingdao University, Qingdao 266000, Shandong, China; [2]Department of Tuberculosis, Affiliated Nantong Hospital of Shanghai University, Nantong 226000, Jiangsu, China

Received September 11, 2024; Accepted January 13, 2025; Epub February 15, 2025; Published February 28, 2025

Abstract: Objectives: To develop a nomogram for the prediction of the new high-grade patterns of invasive non-mucinous adenocarcinoma (INMA) based on the radiomics and clinical features to provide accurate individualized treatment for patients. Methods: We collected patients pathologically diagnosed with INMA at our hospital. The study's endpoint, defined as 'new high-grade', was characterized by the presence of micropapillary patterns at ≥5% or high-grade patterns (including solid, micropapillary, and complex glandular) at ≥20%. Patients were randomly divided into training and validation cohorts in a ratio of 8:2. The region of interest (ROI) of chest plain scan images was sketched using 3D slicer software. The image and clinical features were analyzed by Least Absolute Shrinkage and Selection Operator (LASSO), univariate, and multivariate regression to construct the radiomics signature and nomogram model. The nomogram model was validated using the validation cohort. Results: A total of 226 patients were divided into training (n = 180) and validation (n = 46) cohorts. From the ROI of these patients, 107 image features were extracted. LASSO regression analysis identified 16 image features that were used to construct the radiomics signature. The area under the curve values for the radiomics signature in the training and validation cohorts were 0.803 and 0.772, respectively. The Harrell's concordance index for the model, with 95% confidence intervals (CI), was 0.815 (CI: 0.806-0.824) for the training cohort and 0.802 (CI: 0.761-0.843) for the validation cohort. Conclusions: The radiomics prediction model demonstrates strong predictive capabilities and could serve as a valuable tool for guiding personalized surgical treatment strategies for patients with INMA.

Keywords: Invasive non-mucinous adenocarcinoma, nomogram, radiomics, pathological subtype, lobectomy, sublobar resection

Introduction

Lung adenocarcinoma (LUAD) is the most prevalent form of non-small cell lung cancer (NSCLC). The World Health Organization's (WHO) 2021 classification of thoracic tumors distinguishes LUAD into three subtypes: minimally invasive adenocarcinoma, invasive non-mucinous adenocarcinoma (INMA), and invasive mucinous adenocarcinoma [1]. INMA is further categorized into five subtypes: lepidic, acinar, papillary, solid, and micropapillary. Complex glandular patterns are not explicitly categorized, but they are considered high-grade in conjunction with solid and micropapillary patterns [2]. The International Association for the Study of Lung Cancer (IASLC) Pathology Committee has established a grading system for LUAD based on the predominant histological subtypes and the percentage of high-grade patterns (solid, micropapillary, and complex glandular components) as a basis for prognostic stratification: 1) Grade 1 (Well-differentiated): Tumors predominantly composed of lepidic growth patterns, with no or less than 20% of high-grade subtypes. 2) Grade 2 (Moderately differentiated): Tumors predominantly composed of acinar or papillary patterns, with no more than 20% of high-grade subtypes. 3) Grade 3 (Poorly differentiated): Any tumor with 20% or more of high-grade patterns [3]. This grading system not only reflects the histological characteristics of the tumor but is also closely related to patient prognosis. Recent studies

https://doi.org/10.62347/IHZB9566

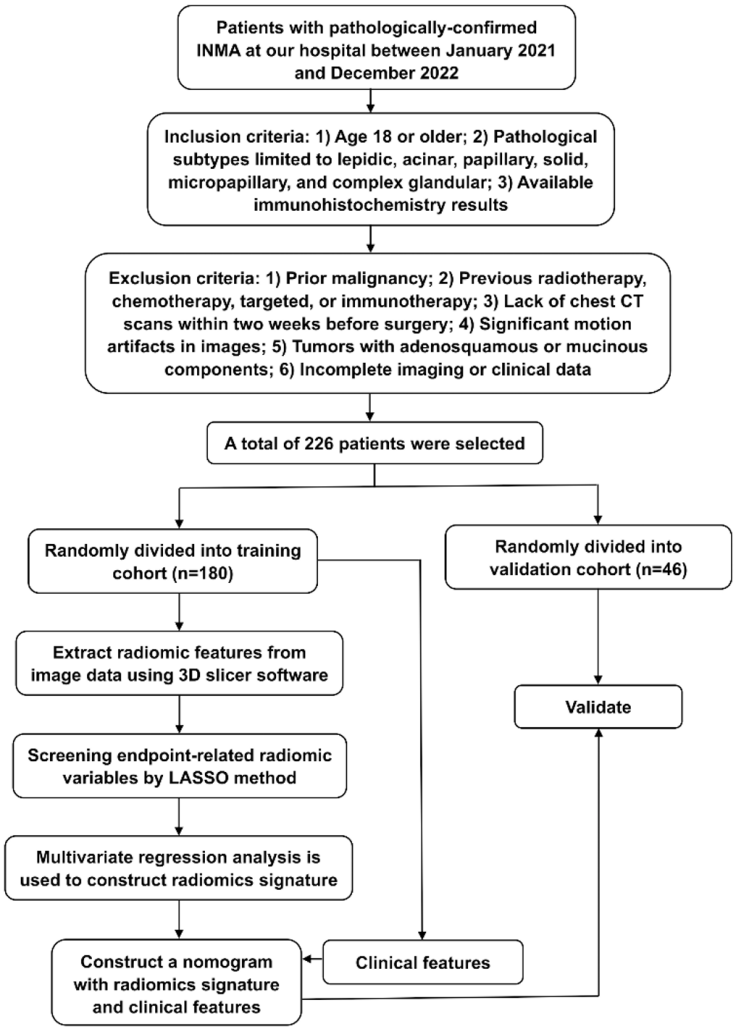

Figure 1. Flowchart of the study.

have revealed that in various histological subtypes of LUAD, the micropapillary component, even with a low proportion, is significantly associated with poor prognosis [4]. This finding has a substantial impact on the long-term survival of patients and the recurrence of tumors.

Radiomics is an emerging technology that extracts a large number of high-throughput features from medical images, transforming image data into a feature space that can be mined, thereby revealing the micro and macro information of diseases. This provides a new perspective for disease diagnosis, efficacy assessment, and prognosis. With the development of artificial intelligence technology, especially the application of deep learning in radiomics, the features extracted from image data have become richer and more accurate.

The study of radiomics in lung cancer prediction is one of the hot topics at the intersection of medical imaging and artificial intelligence. In the latest research, scholars have used advanced deep learning techniques, combined with radiomics features, to construct predictive models to assess the biological characteristics and heterogeneity of tumors, predict treatment response, and monitor disease progression. This is of great significance for the formulation of personalized treatment plans. Radiomics has proven its predictive prowess in various lung tumor assessments, including differentiating benign from malignant tumors [5], forecasting the prognosis of NSCLC [6], anticipating the growth rate of early-stage LUAD [7], and even gauging responses to immunotherapy in advanced NSCLC [8]. However, the predictive significance of radiomics within the IASLC grading system remains unclear. Against this backdrop, we have redefined high-grade patterns and developed a model capable of predicting new high-grade patterns in INMA. This could have profound implications for surgical decision-making processes.

Material and methods

Patient selection

The flowchart of this study is presented in **Figure 1**. A sample size of at least 30 is needed to support statistical models; a sample size of at least 80 is required for the root mean square error of machine learning algorithms to be below 0.01 [9]. This retrospective study was conducted on patients with pathologically confirmed INMA at our hospital between January 2021 and December 2022. The inclusion criteria were specified as follows: 1) Patients must be 18 years of age or older; 2) The pathological subtypes of patients were limited to lepidic, acinar, papillary, solid, micropapillary, and complex glandular subtypes; 3) Immunohistochemistry results for patients must be available. The exclusion criteria were established as fol-

lows: 1) Patients with a prior history of malignant tumors were excluded; 2) Patients who had received radiotherapy, chemotherapy, targeted therapy, or immunotherapy were excluded; 3) Patients who did not have chest computed tomography (CT) images obtained within two weeks preceding surgery were excluded; 4) Patients whose images exhibited significant motion artifacts were excluded; 5) Patients whose tumors contained components such as adenosquamous carcinoma or mucinous adenocarcinoma were excluded; 6) Patients with incomplete imaging or clinical data were excluded. All patients selected for inclusion were randomly assigned to training and validation cohorts, with the ratio of 8:2.

Clinical, imaging, and pathological features

The study collected clinical data on the patients, including age, gender, tumor location, TNM stage, histopathology, pathological subtypes, and immunohistochemistry.

Chest CT was performed on a 64-row GE Optima CT670 scanner (GE Healthcare). The parameters of the CT scanner were as follows: tube voltage, 120 kVp; tube current, 200 mA, modulated automatically; field of view, 360 mm; detector collimation, 0.625 mm; width of the detector, 40 mm; pitch, 0.984; matrix, 512 × 512; section thickness, 1.25 mm; section interval, 1.25 mm.

A thoracic surgeon and a radiologist, each with over 5 years of experience in thoracic imaging, analyzed all plain chest CT images. The initial images were exported in DICOM format and subsequently converted to NIFTI format for segmentation. The ROI was manually sketched using 3D Slicer software version 5.0.3. The ROI needed to avoid the influence of blood vessels, bronchi, pleura, and other tissues. Discrepancies in the ROI were resolved by a radiologist with 10 years of experience in thoracic imaging, who re-sketched the ROI.

In the evaluation of spread through air spaces (STAS), we analyzed INMA samples stained with hematoxylin and eosin as well as those subjected to immunohistochemical staining, utilizing microscopic examination. Our focus was on identifying tumor cells or clusters that manifested as micropapillary clusters, solid cell clusters, or single tumor cells, with particular emphasis on their presence within air spaces located at a distance from the primary tumor margin. Specifically, we employed a criterion of a minimum distance equivalent to one pulmonary acinar interval to ascertain that the observed tumor cells or clusters were located away from the primary tumor margin [10]. Furthermore, we verified that these cells were situated within the normal alveolar cavities and bronchioles, rather than within pseudoglandular or necrotic regions of the tumor. Throughout the evaluation process, we meticulously excluded any potential artifacts to ensure the accuracy of the STAS diagnosis.

The calculation of the Ki-67 index was conducted based on the following method: immunohistochemical staining was performed to assess the distribution of tumor cells. Initially, tissue sections were observed under low magnification to identify areas with uniform tumor cell distribution and optimal staining quality. Subsequently, high magnification was utilized for the purpose of cell counting. A minimum of 10 high-power fields were selected for quantification. The Ki-67 labeling index was calculated using the following formula: Ki-67 Labeling Index = (Number of Ki-67 positive cells/Total number of cells counted) × 100%.

The pathological results were classified into three grades based on the proportion of the components: Low (grade 1), Intermediate (grade 2), and High (grade 3). Pathological subtypes were diagnosed with a 5% increment standard, and the tissue composition of each subtype was recorded from high to low. It is noteworthy that specific ratios of high-grade components were meticulously recorded. Two experienced pathologists who were blinded to clinical information, independently assessed the pathological subtypes, histopathological findings, and immunohistochemical results. In cases where the results were contentious, a third experienced pathologist was brought in to conduct a review.

The study defined the endpoint as the presence of micropapillary patterns ≥5% or high-grade patterns (including solid, micropapillary, and complex glandular) ≥20%.

Construction and validation of the nomogram prediction model

In this study, the primary predictive factors encompass clinical characteristics, radiological

Table 1. Clinical characteristics of subjects

Characteristic	Total (n = 226), (%)	Training cohort (n = 180), (%)	Validation cohort (n = 46), (%)	*P*-value
Age	63.22±9.539	62.99±9.695	64.13±8.943	0.470
Gender				0.969
Male	89 (39.38)	71 (39.44)	18 (39.13)	
Female	137 (60.62)	109 (60.56)	28 (60.87)	
Tumor location				0.099
Right upper lobe	79 (34.96)	59 (32.78)	20 (43.48)	
Right middle lobe	12 (5.31)	10 (5.56)	2 (4.35)	
Right lower lobe	55 (24.34)	48 (26.67)	7 (15.22)	
Left upper lobe	46 (20.35)	40 (22.22)	6 (13.04)	
Left lower lobe	34 (15.04)	23 (12.78)	11 (23.91)	
pT				0.063
T1	214 (94.69)	173 (96.11)	41 (89.13)	
T2	9 (3.98)	6 (3.33)	3 (6.52)	
T3	3 (1.33)	1 (0.56)	2 (4.35)	
pN				0.541
N0	198 (87.61)	159 (88.33)	39 (84.78)	
N1	1 (0.44)	1 (0.56)	0	
N2	16 (7.08)	13 (7.22)	3 (6.52)	
Nx	11 (4.87)	7 (3.89)	4 (8.70)	
pM0	226 (100)	180 (100)	46 (100)	
CT features				
Pleural indentation	69 (30.53)	57 (31.67)	12 (26.09)	0.463
Spiculation or lobulation	99 (43.81)	77 (42.78)	22 (47.83)	0.538
Endpoint	130 (57.52)	99 (55.00)	31 (67.39)	0.129

features, and histopathological features. Secondary predictive factors include gender, age, pleural indentation, spiculation or lobulation signs, pathological subtypes, and immunohistochemistry results. Radiomics characteristics of the training cohort were extracted from an online website (www.home-for-researchers.com). The extracted data underwent cleaning and standardization processes. The Least Absolute Shrinkage and Selection Operator (LASSO) regression analysis was employed to identify the most relevant radiomics features correlated with the endpoint. Univariate logistic analysis assessed the most significant radiomics features in relation to endpoints (P<0.05). A multivariate logistic analysis was conducted to formulate the radiomics signature. The sensitivity, specificity, and accuracy of the signature were appraised using the receiver operating characteristic (ROC) curve and the area under the ROC curve (AUC) value. The radiomics signature, combined with clinical features - gender, age, pleural indentation, and spiculation or lobulation signs - was utilized to develop a nomogram prediction model through multivariate Cox proportional hazards regression analysis. The model's predictive prowess was evaluated using Harrell's concordance index (C-index), 95% confidence interval (CI), and the calibration curve. The validation cohort is utilized to verify the model's effectiveness in predicting new pathological subtypes.

Statistical analysis

Radiomics and clinical features were analyzed using a t-test, chi-square test, or Fisher's exact test based on the distribution characteristics of the data. A *P*-value of <0.05 was considered statistically different. All statistical analyses were performed using the R program (v4.0.3) and SPSS 24 (IBM Corporation).

Results

Cohorts and clinical characteristics

The study included 226 patients, who were allocated randomly into two cohorts: training (n = 180) and test (n = 46). The clinical characteristics are summarized and listed in **Table 1**. The clinical characteristics were comparable between the two cohorts (P>0.05). **Figure 2** illustrates the results of the ROI.

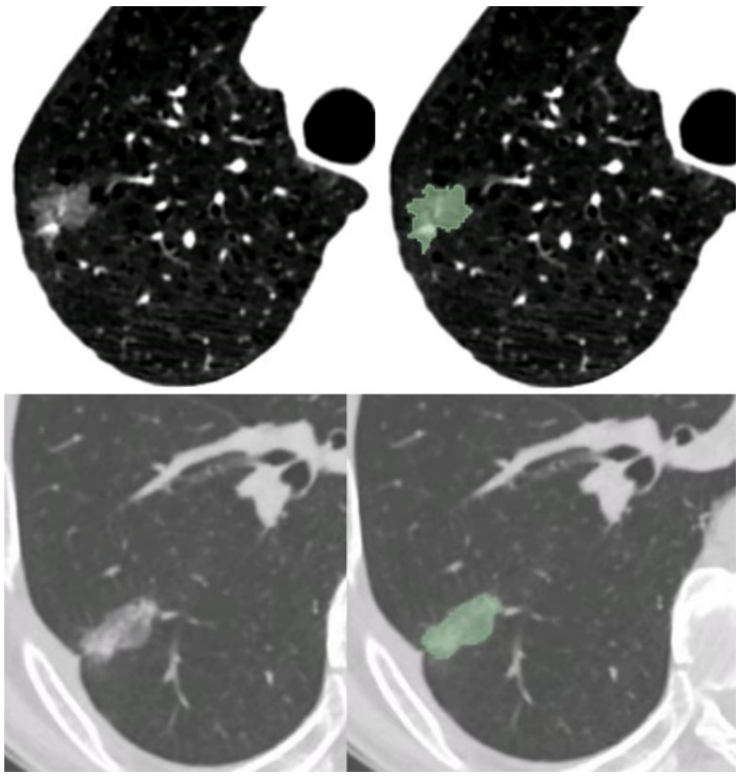

Figure 2. The region of interest (ROI) of the CT images.

Pathological characteristics

The histopathological and immunohistochemical results of 226 patients are listed in **Table 2**. There were no significant differences observed between the two cohorts (P>0.05). The training cohort was divided into two groups based on whether it met the endpoint or not. Tumor STAS and Ki-67 expression were statistically significantly different between the EP and NEP subgroups (P<0.01 for both findings). The subgroups within the validation cohort demonstrated similar tumor STAS results (P<0.01) and Ki-67 expressions (P = 0.037), as shown in **Table 3**. This supports our hypothesis that even no less than 5% of micropapillary components in pathological subtypes will lead to higher invasiveness and worse prognosis.

Radiomics features and signature

A total of 107 features were extracted from the ROI of 226 patients, of which 16 features, including original_shape_(Elongation, Flatness, Maximum2DDiameterColumn, Maximum2DDiameterRow), original_firstorder_(Energy, Maximum, Minimum, Skewness, TotalEnergy), original_glcm_(Imc1, JointEntropy), original_gldm_(DependenceVariance, LargeDependenceLowGrayLevelEmphasis), original_glszm_(SizeZoneNonUniformityNormalized, SmallAreaLow-GrayLevelEmphasis), and original_ngtdm_Contrast, were screened out by LASSO regression analysis to construct a radiomics signature. **Figure 3** depicts the forest plot of the univariate Cox analysis. The radiomics signature score was calculated using the following formula: Radiomics score = 0.45 + (0.577) × shape_Maximum2DDiameterColumn + (0.241) × firstorder_Maximum + (-0.06) × firstorder_Skewness + (-0.268) × glcm_Imc1+(-1.719) × glcm_JointEntropy+(-0.426) × gldm_DependenceVariance + (-0.277) × glszm_SizeZoneNonUniformityNormalized + (-0.509) × glszm_SmallAreaLowGrayLevelEmphasis + (0.577) × ngtdm_Contrast. **Figure 4** presents the ROC curves, with AUC values of 0.803 for the training cohort and 0.772 for the validation cohort, respectively.

Construction and validation of the nomogram model

The radiomics signature and clinical features (gender, age, pleural indentation, and spiculation or lobulation sign) were used to construct a nomogram prediction model (**Figure 5**). The C-index of the training and validation cohorts is 0.815 (95% CI: 0.806-0.824) and 0.802 (95% CI: 0.761-0.843), respectively. The calibration curves of the nomogram are displayed in **Figure 4**.

Discussion

In 2020, the IASLC proposed a new grading system for invasive pulmonary adenocarcinoma (IAC) [3]. Combined with the classification of lung tumors by WHO in 2021, we believed that this grading system is more suitable for INMA [1]. Nonetheless, the complex glandular pattern, encompassing cribriform and fused glands, remains excluded from the INMA clas-

Table 2. Pathological characteristics of subjects

Characteristic	Total (n = 226), (%)	Training cohort (n = 180), (%)	Validation cohort (n = 46), (%)	*P*-value
Grade				0.710
Low (grade 1)	25 (11.06)	20 (11.11)	5 (10.87)	
Intermediate (grade 2)	124 (54.87)	101 (56.11)	23 (50.00)	
High (grade 3)	77 (34.07)	59 (32.78)	18 (39.13)	
STAS	70 (30.97)	53 (29.44)	17 (36.96)	0.325
EGFR (+)	215 (95.13)	170 (94.44)	45 (97.83)	0.570
P53 (+)	123 (54.42)	102 (56.67)	21 (45.65)	0.181
Ki-67	0.171±0.153	0.169±0.151	0.181±0.164	0.642
Group				0.447
Met the endpoint	130 (57.52)	99 (55.00)	31 (67.39)	
STAS (+)	68	51	17	
STAS (-)	62	48	14	
Not met the endpoint				
STAS (+)	2	2	0	
STAS (-)	94	79	15	

STAS: spread through air spaces.

Table 3. The correlation among endpoint, tumor STAS, and Ki-67

Groups	Total (n = 226), (%)	*P*-value	Training cohort (n = 180), (%)	*P*-value	Validation cohort (n = 46), (%)	*P*-value
STAS		**		**		**
(+) (EP)	68 (30.09)		51 (28.33)		17 (36.96)	
(-) (EP)	62 (27.43)		48 (26.67)		14 (30.43)	
(+) (NEP)	2 (0.89)		2 (1.11)		0	
(-) (NEP)	94 (41.59)		79 (43.89)		15 (32.61)	
Ki-67		**		**		0.037
EP	130 (57.52)		99 (55.00)		31 (67.39)	
Ki-67	0.221±0.176		0.225±0.173		0.208±0.189	
NEP	96 (42.48)		81 (45.00)		15 (32.61)	
Ki-67	0.105±0.074		0.101±0.074		0.125±0.073	

EP: endpoint group; NEP: non-endpoint group; **: P<0.01.

sification. A previous study showed that cribriform-predominant tumors have a poor prognosis similar to solid- and micropapillary-predominant subtypes [11]. Warth et al. found that the overall survival (OS) of patients with cribriform-predominant tumors (mean OS: 62.7 months) was between acinar-predominant (mean OS: 71.3 months) and solid-predominant (mean OS: 54.5 months) subtypes. However, the disease-free survival (DFS) (mean DFS: 36.9 months) was the worst of all patterns [12]. Moreira et al. showed that fused gland-predominant tumors had similar DFS curves compared with cribriform-, solid-, and micropapillary-predominant tumors (P = 0.56) [2]. Collectively, these findings support the use of complex glandular as a high-grade indicator.

In IAC, tumors with micropapillary- and solid-predominant patterns are associated with poor post-recurrence survival [13] and DFS [14]. The micropapillary pattern, in particular, stands out as an independent predictor of OS [14] as well as the presence of occult mediastinal lymph node metastasis (pN2) [15]. Song et al. discovered that patients with a micropapillary component <5% had a lower TNM stage, whereas those with 5% or more micropapillary pattern experienced more frequent N2 disease [16]. Nitadori et al. found that limited resection was more likely to relapse than lobectomy in patients with a micropapillary component ≥5% [17]. Even in the early stages of LUAD, patient outcomes are significantly associated with the proportion of high-grade tumor patterns [3, 18].

Although complete pathological results for lymph nodes were unavailable for 11 patients due to factors such as final pathology upgrades

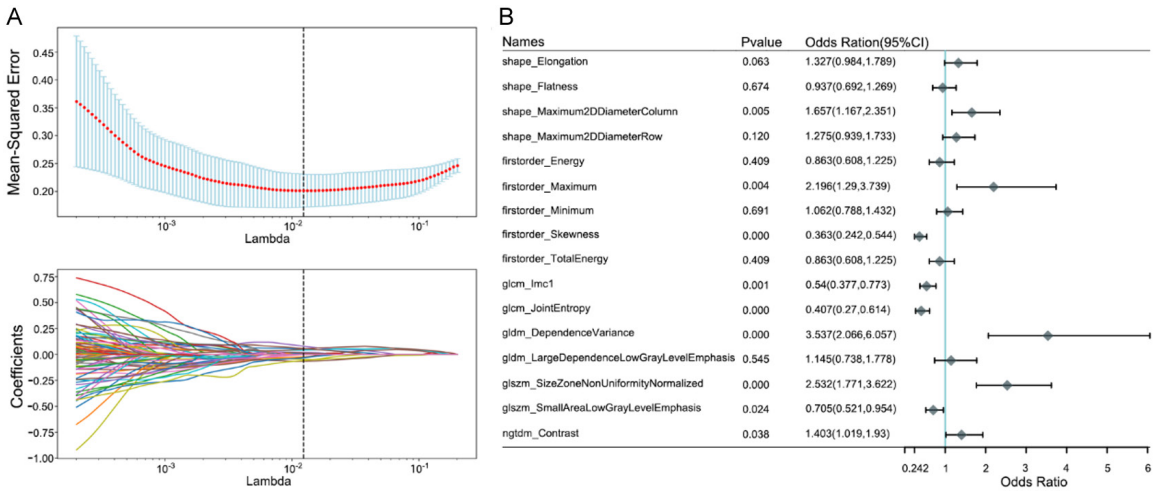

Figure 3. Least Absolute Shrinkage and Selection Operator (LASSO) regression analysis (A) and forest plots (B) of the radiomics signature in the training cohorts.

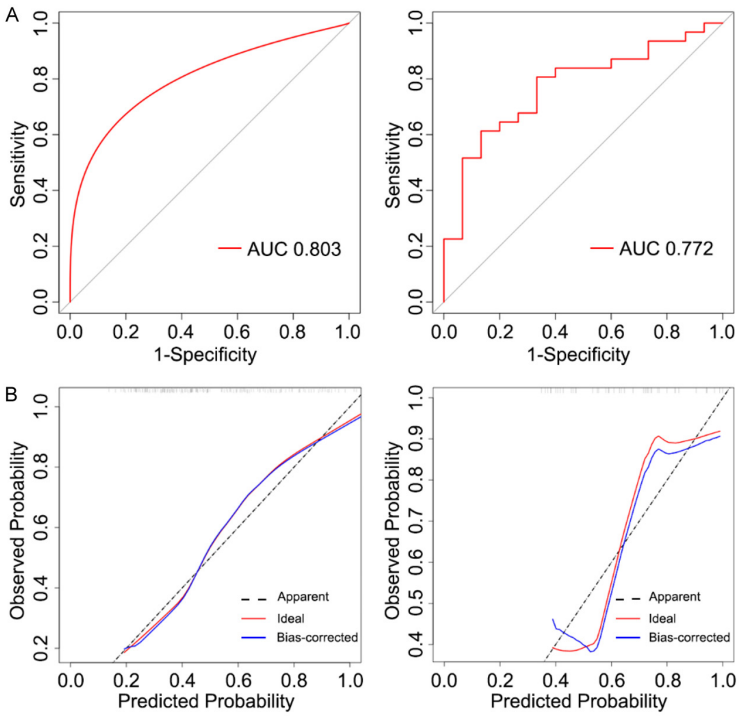

Figure 4. The receiver operating characteristic (ROC) curves and area under the curve (AUC) values of the training and validation cohorts (A). Calibration curves of the training and validation cohorts (B).

or inadequate lymph node sampling, these omissions did not impact the study's endpoint. Consequently, we included the data from these 11 patients in our analysis. Our findings indicate that the EP group across the total, training, and validation cohorts exhibited a higher incidence of tumor STAS and Ki-67 expression compared to the NEP group. Both STAS and Ki-67 have been identified as poor prognostic indicators for high-grade patterns in numerous studies [3, 19-21]. Our results align with these findings, reinforcing the relevance of our study's endpoint. The nomogram prediction model, based on these criteria, demonstrated robust predictive accuracy.

Radiomics is increasingly recognized as a pivotal component in the diagnostic and therapeutic processes for NSCLC. Through a comprehensive analysis of the macroscopic morphological characteristics and imaging data of pulmonary nodules, radiomics provides essential non-invasive support for the differential diagnosis of benign versus malignant pulmonary nodules. Within the domain of pathology, the application of radiomics has evolved beyond distinguishing pathological subtypes of LUAD to include the prediction of occult metastases in mediastinal lymph nodes [22], brain metastases [23], STAS [24], and the mutation status of the epidermal growth factor receptor gene [25]. Furthermore, radiomics demonstrates significant potential in prognosticating outcomes for NSCLC patients.

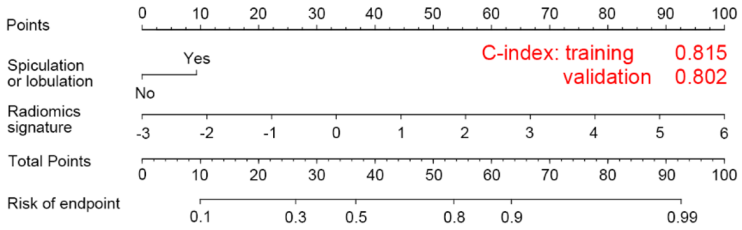

Figure 5. Nomogram prediction model and Harrell's concordance index (C-index) of training and validation cohorts.

It can, for instance, predict the likelihood of early-stage NSCLC patients benefiting from immunotherapy [26], evaluate the risk of recurrence following surgical intervention for stage I LUAD [27], and monitor variations in the neutrophil-to-lymphocyte ratio post-radiotherapy in locally advanced NSCLC [28]. Additionally, radiomics can forecast the probability of radiation pneumonitis in NSCLC patients undergoing radiotherapy [29] and assess disease progression in early-stage NSCLC following stereotactic ablative radiotherapy [30]. This series of research findings enhances our comprehension of the biological characteristics of NSCLC and contributes to the development of more precise diagnostic strategies and personalized treatment plans for patients. Previous surgical procedures for peripheral small-sized LUAD depended on the results of an intraoperative frozen section [31]. However, the potential for postoperative pathological upgrades, influenced by varying pathologist expertise, was not uncommon. The release of findings from trials such as JCOG0201/0804/0802/1211 marked a shift towards imaging-guided surgical practices. Yet, debates persist, particularly regarding JCOG0802/WJOG4607L, where segmentectomy showed superior OS compared to lobectomy, though with a higher rate of local relapse [32]. Local recurrence is influenced by factors like tumor STAS, the prevalence of high-grade tumor patterns, and the proximity between tumor margins and resection boundaries. Unfortunately, JCOG0802 lacked detailed insights into these factors. The CALGB140503 study demonstrated that the DFS, OS, and locoregional or distant recurrence of sublobar resection were not inferior to those of lobectomy in stage I NSCLC patients with peripheral tumor that is ≤2 cm and negative hilar and mediastinal lymph nodes [33]. However, no further information on STAS and pathological subtypes was reported in this study. Consequently, integrating findings from these studies with radiomics-based predictions of high-grade tumor patterns could inform personalized treatment strategies.

This study acknowledges several inherent limitations. Firstly, variations in pathologists' expertise may have introduced bias into the study outcomes. Secondly, the predictive model developed here has yet to be cross-validated with datasets from other medical institutions. Thirdly, the model's applicability necessitates further confirmation through larger-scale, prospective studies to ensure its broader validity. Lastly, the study's patient follow-up duration was relatively brief, precluding the availability of comprehensive long-term outcome data.

In summary, our radiomics-based nomogram model successfully predicts new high-grade patterns in INMA. Combined with the results of JCOG0201/0804/0802 and CALGB140503, this model could be used to guide clinical decisions and individualized surgical treatment strategies for patients with pulmonary nodules.

Disclosure of conflict of interest

None.

Address correspondence to: Yingying Zhang, Department of Tuberculosis, Affiliated Nantong Hospital of Shanghai University, Nantong 226000, Jiangsu, China. E-mail: 1895139@qq.com

References

[1] Nicholson AG, Tsao MS, Beasley MB, Borczuk AC, Brambilla E, Cooper WA, Dacic S, Jain D, Kerr KM, Lantuejoul S, Noguchi M, Papotti M, Rekhtman N, Scagliotti G, van Schil P, Sholl L, Yatabe Y, Yoshida A and Travis WD. The 2021 WHO classification of lung tumors: impact of advances since 2015. J Thorac Oncol 2022; 17: 362-387.

[2] Moreira AL, Joubert P, Downey RJ and Rekhtman N. Cribriform and fused glands are patterns of high-grade pulmonary adenocarcinoma. Hum Pathol 2014; 45: 213-220.

[3] Moreira AL, Ocampo PSS, Xia Y, Zhong H, Russell PA, Minami Y, Cooper WA, Yoshida A, Bubendorf L, Papotti M, Pelosi G, Lopez-Rios F, Kunitoki K, Ferrari-Light D, Sholl LM, Beasley

MB, Borczuk A, Botling J, Brambilla E, Chen G, Chou TY, Chung JH, Dacic S, Jain D, Hirsch FR, Hwang D, Lantuejoul S, Lin D, Longshore JW, Motoi N, Noguchi M, Poleri C, Rekhtman N, Tsao MS, Thunnissen E, Travis WD, Yatabe Y, Roden AC, Daigneault JB, Wistuba II, Kerr KM, Pass H, Nicholson AG and Mino-Kenudson M. A grading system for invasive pulmonary adenocarcinoma: a proposal from the International Association for the Study of Lung Cancer Pathology Committee. J Thorac Oncol 2020; 15: 1599-1610.

[4] Qian F, Yang W, Wang R, Xu J, Wang S, Zhang Y, Jin B, Yu K and Han B. Prognostic significance and adjuvant chemotherapy survival benefits of a solid or micropapillary pattern in patients with resected stage IB lung adenocarcinoma. J Thorac Cardiovasc Surg 2018; 155: 1227-1235, e1222.

[5] Wang HJ, Lin MW, Chen YC, Chen LW, Hsieh MS, Yang SM, Chen HF, Wang CW, Chen JS, Chang YC and Chen CM. A radiomics model can distinguish solitary pulmonary capillary haemangioma from lung adenocarcinoma. Interact Cardiovasc Thorac Surg 2022; 34: 369-377.

[6] Bortolotto C, Lancia A, Stelitano C, Montesano M, Merizzoli E, Agustoni F, Stella G, Preda L and Filippi AR. Radiomics features as predictive and prognostic biomarkers in NSCLC. Expert Rev Anticancer Ther 2021; 21: 257-266.

[7] Tan M, Ma W, Sun Y, Gao P, Huang X, Lu J, Chen W, Wu Y, Jin L, Tang L, Kuang K and Li M. Prediction of the growth rate of early-stage lung adenocarcinoma by radiomics. Front Oncol 2021; 11: 658138.

[8] He B, Dong D, She Y, Zhou C, Fang M, Zhu Y, Zhang H, Huang Z, Jiang T, Tian J and Chen C. Predicting response to immunotherapy in advanced non-small-cell lung cancer using tumor mutational burden radiomic biomarker. J Immunother Cancer 2020; 8: e000550.

[9] Gillies RJ, Kinahan PE and Hricak H. Radiomics: images are more than pictures, they are data. Radiology 2016; 278: 563-577.

[10] Kadota K, Nitadori JI, Sima CS, Ujiie H, Rizk NP, Jones DR, Adusumilli PS and Travis WD. Tumor spread through air spaces is an important pattern of invasion and impacts the frequency and location of recurrences after limited resection for small stage I lung adenocarcinomas. J Thorac Oncol 2015; 10: 806-814.

[11] Kadota K, Yeh YC, Sima CS, Rusch VW, Moreira AL, Adusumilli PS and Travis WD. The cribriform pattern identifies a subset of acinar predominant tumors with poor prognosis in patients with stage I lung adenocarcinoma: a conceptual proposal to classify cribriform predominant tumors as a distinct histologic subtype. Mod Pathol 2014; 27: 690-700.

[12] Warth A, Muley T, Kossakowski C, Stenzinger A, Schirmacher P, Dienemann H and Weichert W. Prognostic impact and clinicopathological correlations of the cribriform pattern in pulmonary adenocarcinoma. J Thorac Oncol 2015; 10: 638-644.

[13] Hung JJ, Yeh YC, Jeng WJ, Chien HC, Wu YC, Chou TY and Hsu WH. Prognostic factors of survival after recurrence in patients with resected lung adenocarcinoma. J Thorac Oncol 2015; 10: 1328-1336.

[14] Cha MJ, Lee HY, Lee KS, Jeong JY, Han J, Shim YM and Hwang HS. Micropapillary and solid subtypes of invasive lung adenocarcinoma: clinical predictors of histopathology and outcome. J Thorac Cardiovasc Surg 2014; 147: 921-928, e922.

[15] Yeh YC, Kadota K, Nitadori J, Sima CS, Rizk NP, Jones DR, Travis WD and Adusumilli PS. International Association for the Study of Lung Cancer/American Thoracic Society/European Respiratory Society classification predicts occult lymph node metastasis in clinically mediastinal node-negative lung adenocarcinoma. Eur J Cardiothorac Surg 2016; 49: e9-e15.

[16] Song SH, Park H, Lee G, Lee HY, Sohn I, Kim HS, Lee SH, Jeong JY, Kim J, Lee KS and Shim YM. Imaging phenotyping using radiomics to predict micropapillary pattern within lung adenocarcinoma. J Thorac Oncol 2017; 12: 624-632.

[17] Nitadori J, Bograd AJ, Kadota K, Sima CS, Rizk NP, Morales EA, Rusch VW, Travis WD and Adusumilli PS. Impact of micropapillary histologic subtype in selecting limited resection vs lobectomy for lung adenocarcinoma of 2cm or smaller. J Natl Cancer Inst 2013; 105: 1212-1220.

[18] Wang Y, Yang X, Liu B, Yan S, Liu M, Li X, Li S, Lv C, Ma Y, Zhou L, Song Z, Xv W, Yang Y, Lin D and Wu N. Percentage of newly proposed high-grade patterns is associated with prognosis of pathological T1-2N0M0 lung adenocarcinoma. Ann Surg Oncol 2022; [Epub ahead of print].

[19] Gross DJ, Hsieh MS, Li Y, Dux J, Rekhtman N, Jones DR, Travis WD and Adusumilli PS. Spread through air spaces (STAS) in non-small cell lung carcinoma: evidence supportive of an in vivo phenomenon. Am J Surg Pathol 2021; 45: 1509-1515.

[20] Li Z, Li F, Pan C, He Z, Pan X, Zhu Q, Wu W and Chen L. Tumor cell proliferation (Ki-67) expression and its prognostic significance in histological subtypes of lung adenocarcinoma. Lung Cancer 2021; 154: 69-75.

[21] Lee JS, Kim EK, Kim M and Shim HS. Genetic and clinicopathologic characteristics of lung

adenocarcinoma with tumor spread through air spaces. Lung Cancer 2018; 123: 121-126.
[22] Zhong Y, Yuan M, Zhang T, Zhang YD, Li H and Yu TF. Radiomics approach to prediction of occult mediastinal lymph node metastasis of lung adenocarcinoma. AJR Am J Roentgenol 2018; 211: 109-113.
[23] Chen A, Lu L, Pu X, Yu T, Yang H, Schwartz LH and Zhao B. CT-based radiomics model for predicting brain metastasis in category T1 lung adenocarcinoma. AJR Am J Roentgenol 2019; 213: 134-139.
[24] Han X, Fan J, Zheng Y, Ding C, Zhang X, Zhang K, Wang N, Jia X, Li Y, Liu J, Zheng J and Shi H. The value of CT-based radiomics for predicting spread through air spaces in stage IA lung adenocarcinoma. Front Oncol 2022; 12: 757389.
[25] Li S, Ding C, Zhang H, Song J and Wu L. Radiomics for the prediction of EGFR mutation subtypes in non-small cell lung cancer. Med Phys 2019; 46: 4545-4552.
[26] Cousin F, Louis T, Dheur S, Aboubakar F, Ghaye B, Occhipinti M, Vos W, Bottari F, Paulus A, Sibille A, Vaillant F, Duysinx B, Guiot J and Hustinx R. Radiomics and delta-radiomics signatures to predict response and survival in patients with non-small-cell lung cancer treated with immune checkpoint inhibitors. Cancers (Basel) 2023; 15: 1968.
[27] Lan H, Wei C, Xu F, Yang E, Lu D, Feng Q and Li T. 2.5D peritumoural radiomics predicts postoperative recurrence in stage I lung adenocarcinoma. Front Oncol 2024; 14: 1382815.
[28] Hou R, Xia W, Zhang C, Shao Y, Zhu X, Feng W, Zhang Q, Yu W, Fu X and Zhao J. Dosiomics and radiomics improve the prediction of post-radiotherapy neutrophil-lymphocyte ratio in locally advanced non-small cell lung cancer. Med Phys 2024; 51: 650-661.
[29] Evin C, Razakamanantsoa L, Gardavaud F, Papillon L, Boulaala H, Ferrer L, Gallinato O, Colin T, Moussa SB, Harfouch Y, Foulquier JN, Guillerm S, Bibault JE, Huguet F, Wagner M and Rivin Del Campo E. Clinical, dosimetric and radiomic features predictive of lung toxicity after (chemo)radiotherapy. Clin Lung Cancer 2025; 26: 93-103, e1.
[30] Yang H, Wang L, Shao G, Dong B, Wang F, Wei Y, Li P, Chen H, Chen W, Zheng Y, He Y, Zhao Y, Du X, Sun X, Wang Z, Wang Y, Zhou X, Lai X, Feng W, Shen L, Qiu G, Ji Y, Chen J, Jiang Y, Liu J, Zeng J, Wang C, Zhao Q, Yang X, Hu X, Ma H, Chen Q, Chen M, Jiang H and Xu Y. A combined predictive model based on radiomics features and clinical factors for disease progression in early-stage non-small cell lung cancer treated with stereotactic ablative radiotherapy. Front Oncol 2022; 12: 967360.
[31] Liu S, Wang R, Zhang Y, Li Y, Cheng C, Pan Y, Xiang J, Zhang Y, Chen H and Sun Y. Precise diagnosis of intraoperative frozen section is an effective method to guide resection strategy for peripheral small-sized lung adenocarcinoma. J Clin Oncol 2016; 34: 307-313.
[32] Saji H, Okada M, Tsuboi M, Nakajima R, Suzuki K, Aokage K, Aoki T, Okami J, Yoshino I, Ito H, Okumura N, Yamaguchi M, Ikeda N, Wakabayashi M, Nakamura K, Fukuda H, Nakamura S, Mitsudomi T, Watanabe SI and Asamura H; West Japan Oncology Group and Japan Clinical Oncology Group. Segmentectomy versus lobectomy in small-sized peripheral non-small-cell lung cancer (JCOG0802/WJOG4607L): a multicentre, open-label, phase 3, randomised, controlled, non-inferiority trial. Lancet 2022; 399: 1607-1617.
[33] Altorki N, Wang X, Kozono D, Watt C, Landrenau R, Wigle D, Port J, Jones DR, Conti M, Ashrafi AS, Liberman M, Yasufuku K, Yang S, Mitchell JD, Pass H, Keenan R, Bauer T, Miller D, Kohman LJ, Stinchcombe TE and Vokes E. Lobar or sublobar resection for peripheral stage IA non-small-cell lung cancer. N Engl J Med 2023; 388: 489-498.